

# Electronic Raman scattering in the single-CuO<sub>2</sub> layered superconductor Tl<sub>2</sub>Ba<sub>2</sub>CuO<sub>6+δ</sub>

L.V. Gasparov

2. *Physikalisches Institut, RWTH-Aachen, 52056 Aachen, Germany*  
*Institute for Solid State Physics, 142432, Chernogolovka, Moscow district, Russia*

P. Lemmens

2. *Physikalisches Institut, RWTH-Aachen, 52056 Aachen, Germany*

M. Brinkmann

2. *Physikalisches Institut, RWTH-Aachen, 52056 Aachen, Germany*

N.N. Kolesnikov

*Institute for Solid State Physics 142432, Chernogolovka, Moscow district, Russia*

G. Güntherodt

2. *Physikalisches Institut, RWTH-Aachen, 52056 Aachen, Germany*

(October 6, 2017)

Electronic Raman scattering in Tl<sub>2</sub>Ba<sub>2</sub>CuO<sub>6+δ</sub> (Tl-2201) has been investigated in order to test whether the scattering cross-section in high temperature superconductors depends on the number of CuO<sub>2</sub>-planes, i.e. sheets or specific details of the Fermi surface. The polarized Raman spectra have been measured in different scattering geometries for temperatures above and below T<sub>c</sub>. The spectral features of Tl-2201 with one CuO<sub>2</sub>-plane per unit cell are found to be similar to Tl<sub>2</sub>Ba<sub>2</sub>Ca<sub>2</sub>Cu<sub>3</sub>O<sub>10</sub> with three CuO<sub>2</sub> planes and those of other high temperature superconductors with several CuO<sub>2</sub>-planes per unit cell. The peak in the B<sub>1g</sub> symmetry component of the scattering intensity is found at 460cm<sup>-1</sup> (T<sub>c</sub>=90K), or 430cm<sup>-1</sup> (T<sub>c</sub>=80K). The B<sub>1g</sub> peak positions scale with T<sub>c</sub>, and correspond to 2Δ/k<sub>B</sub>T<sub>c</sub> = 7.6 ± 0.4. The temperature dependence of the B<sub>1g</sub> scattering component of Tl-2201 (T<sub>c</sub>=80K and 90K) reveals a deviation from BCS behavior. The experimental data are in qualitative agreement with the calculations of Devereaux and Einzel based on the d<sub>x<sup>2</sup>-y<sup>2</sup></sub>-wave symmetry of the order parameter used in the description of the Raman scattering cross section.

74.25.Gz, 74.72.Fq, 78.30.-j

## I. INTRODUCTION

Since the discovery of high temperature superconductors (HTSC), the pairing mechanism and the symmetry of the order parameter in these compounds are key questions at stake<sup>1,2</sup>. There are several experimental techniques which are able to address this problem. The experiments on quasiparticle tunneling<sup>3</sup>, the linear temperature dependence of the penetration depth<sup>4</sup>, the NMR and NQR measurements<sup>5,6</sup>, and angular resolved photoemission experiments in Bi<sub>2</sub>Sr<sub>2</sub>CaCu<sub>2</sub>O<sub>8</sub><sup>7,8</sup> have yielded results consistent with *d*-wave pairing. On the other hand, quasiparticle tunneling, the exponential temperature dependence of the penetration depth, as well as the measurements of the electronic Raman scattering in Nd<sub>2-x</sub>Ce<sub>x</sub>CuO<sub>4</sub> are consistent with s-wave pairing<sup>9-11</sup>. The measurements of the magnetic field dependence of the dc-SQUID (YBaCuO-Au-Pb arrangement)<sup>12</sup> clearly indicated d-wave behavior, while the experiments on single Josephson-junction Pb-YBCO<sup>13</sup> showed s-type behavior. So while the experimental evidence in favor of d-wave symmetry of the order parameter continuously grows, there is still no final consensus about it.

Raman scattering is a powerful tool to address the problem of the symmetry of the order parameter. It allows to probe the symmetry of the scattering tensor by simply choosing different polarization directions of the incident and scattered light. From the investigations of the Raman scattering in conventional superconductors it is known that the superconducting transition manifests itself in a renormalization of the electronic Raman scattering intensity below T<sub>c</sub>. It was found for Nb<sub>3</sub>Sn and V<sub>3</sub>Si<sup>14,15</sup> that normalized Raman spectra of these compounds show for temperatures below T<sub>c</sub> a peak associated with the pair breaking process at the energy 2Δ, together with a strong decrease of the scattering intensity at frequencies lower than 2Δ. In high temperature superconductors, the first measurements of electronic Raman scattering were reported in Refs. 16–19. But in this case the behavior of the electronic scattering differs from that in conventional superconductors: A pair breaking peak develops in the spectra below T<sub>c</sub>, but the scattering intensity at frequencies below 2Δ does not show the usual sharp decrease. Instead, a monotonic decrease

toward zero frequency is found. Moreover, for different symmetry components ( $A_{1g}$ ,  $B_{1g}$  and  $B_{2g}$ ) the renormalization of the scattering intensity for  $T < T_c$  is different and they exhibit peaks at different frequencies<sup>18–27,29,30</sup>. These facts have been explained by Devereaux et al.<sup>26,27</sup> in terms of  $d_{x^2-y^2}$ -wave pairing. Their calculations of the scattering cross-section have been performed for a cylindrical single-sheeted Fermi surface in the framework of the kinetic equation approach. The symmetry of the crystal was taken into account through calculating the Raman vertex, which was expanded in terms of a complete set of crystal harmonics defined on the Fermi surface. It was found that nontrivial coupling between the Raman vertex and an assumed strongly anisotropic energy gap leads to the strong symmetry dependence of the scattering intensity. The calculations<sup>26,27</sup> predict specific symmetry dependencies of the low frequency scattering as well as the peak positions for the different symmetry components of the electronic Raman scattering at temperatures below  $T_c$ . The  $A_{1g}$  peak position is sensitive to the parameters of the model calculation. It will appear below  $B_{1g}$  peak position while with some parameters it may also appear at the  $B_{1g}$  peak position. Nevertheless there is one set of parameters which can perfectly reproduce the experimental data<sup>28</sup>. Later on this model was criticized by Krantz and Cardona<sup>29,30</sup>. Their calculations<sup>30</sup> are based on the general description of the Raman scattering cross-section through the inverse effective mass tensor. In case of the multisheeted Fermi surface, (e.g. several  $\text{CuO}_2$  planes per unit cell in HTSC) polarization dependent Raman efficiencies are determined by the averages of the corresponding effective mass fluctuations. The authors of Ref. 30 used the effective masses from LDA band structure calculations for  $\text{YBa}_2\text{Cu}_3\text{O}_7$  to determine the Raman scattering cross-section. They found that it contradicts the experimental results if one uses only d-wave pairing for a multisheeted Fermi surface of  $\text{YBa}_2\text{Cu}_3\text{O}_7$ . An explanation was given by assuming different types of the order parameter on different sheets of the Fermi surface. For a single-sheeted Fermi surface (i.e. one  $\text{CuO}_2$ -plane per unit cell) no mass fluctuations should occur. Therefore in the framework of the effective mass fluctuation approach, the  $A_{1g}$  scattering component will be nearly totally screened and should peak at the same position where the  $B_{1g}$  scattering component ( $2\Delta_{max}$ ). Therefore straightforward measurements of the electronic Raman scattering in single- $\text{CuO}_2$  layered high-temperature superconductors (Tl-2201, La-214, Bi-2201, (Nd,Ce)-214) should clarify this controversial point.

Tl-2201 has the highest  $T_c$  (up to 110K)<sup>31</sup> among the above mentioned single- $\text{CuO}_2$  layered compounds. Therefore all effects due to the gap opening are expected in the range of  $300\text{-}600\text{cm}^{-1}$ , and they should not be obscured due to the Rayleigh scattering at small wavenumbers. Nevertheless, Raman measurements in only one pure scattering geometry ( $B_{1g}$ ) are known<sup>23,32</sup> for this compound, which showed<sup>23</sup> besides a  $T_c=80\text{K}$  two additional transitions at 100 and 125K, which can be indicative of the Tl-2212 and Tl-2223 phases.

These facts lead us to reinvestigate the electronic Raman scattering in the Tl-based high temperature superconductor Tl-2201 (with different oxygen content) with one  $\text{CuO}_2$ -plane per unit cell. The comparison with the results of electronic Raman scattering experiments reported for the high temperature superconductors with several  $\text{CuO}_2$ -planes should clarify whether the multiband scattering is indeed important. We should mention that similar experiments on the single layered compound (La-214) were already carried out<sup>25</sup>. Nevertheless, in the framework of comparison of the compounds with different number of  $\text{CuO}_2$ -planes the measurements on Tl-2201 are more favourable due to its high  $T_c$ .

## II. EXPERIMENT

The investigated single crystals of  $\text{Tl}_2\text{Ba}_2\text{CuO}_{6+\delta}$  (Tl-2201) had the shape of rectangular platelets with the size of approximately  $2\text{x}2\text{x}0.2\text{ mm}^3$ . The two crystals investigated were characterized by a SQUID magnetometer.  $T_c$  was found to be  $90\pm 3\text{ K}$  and  $80\pm 5\text{ K}$ . The crystals are slightly underdoped. It is known<sup>33</sup> that differences in  $T_c$  in Tl-2201 compound originate from different oxygen concentrations. These crystals can be over- as well as underdoped. The heavily oxygen doped crystals show a metallic type of conductivity<sup>33</sup> and do not show a superconducting transition. The orientation of the tetragonal crystals was controlled by X-ray diffraction.

Raman measurements were performed on "as grown" surfaces of the freshly prepared crystals. This is very important, because the crystal surface of Tl-based superconductors as well as of all high temperature superconductors is very sensitive to long exposure to air and especially to humid atmosphere. For the Raman measurements a DILOR XY triple spectrometer combined with a nitrogen cooled CCD detector was used. All Raman data were obtained at nearly backscattering geometry. The photon excitation was provided by the 488-nm line of an  $\text{Ar}^+$  ion laser with laser power equal to  $15\text{W}/\text{cm}^2$ . The estimated additional heating did not exceed 5K.

### III. EXPERIMENTAL RESULTS

All measurements were performed with the polarization of the incident and scattered light parallel to the basal plane of the crystal, i.e. the CuO<sub>2</sub>-planes. It was possible to measure the A<sub>1g</sub>, B<sub>1g</sub>, and B<sub>2g</sub> symmetry components of the Raman scattering cross-section. In addition to the previously published phonon peaks ( $\approx 123\text{cm}^{-1}$ ,  $\approx 169\text{cm}^{-1}$ ,  $\approx 490\text{cm}^{-1}$ ,  $\approx 590\text{cm}^{-1}$ ,  $\approx 610\text{cm}^{-1}$ )<sup>34,35</sup> we have detected some additional phonons ( $\approx 240\text{cm}^{-1}$ ,  $\approx 300\text{cm}^{-1}$ ,  $\approx 330\text{cm}^{-1}$ ,  $\approx 375\text{cm}^{-1}$ ) which we believe are the defect induced infrared active phonons. For all scattering geometries the spectra for temperatures well below T<sub>c</sub> were divided by the spectra just above T<sub>c</sub> in order to emphasize the redistribution of the scattering intensity in the superconducting state compared to the normal state. The results of the electronic Raman scattering in the crystals of Tl-2201 (T<sub>c</sub>=80K,90K) are shown on Figs. 1-5. In the crystal with T<sub>c</sub>=80K the B<sub>1g</sub> scattering component measured in X'Y' configuration shows a well-defined peak at  $430\pm 15\text{cm}^{-1}$  (Fig. 1a). The X' and Y' axes are rotated by 45° with respect to the crystal X and Y axes, respectively, which are parallel to the crystallographic axes. The B<sub>2g</sub> scattering component in Fig. 1b is less intense, but shows also a broad maximum with an average frequency of  $380\pm 35\text{cm}^{-1}$ . Raman spectra in the X'X' and XX geometries are presented in Fig. 2a and b, showing spectra of A<sub>1g</sub> + B<sub>2g</sub> and A<sub>1g</sub> + B<sub>1g</sub> scattering components, respectively. In order to evaluate the A<sub>1g</sub> scattering component we subtracted the B<sub>1g</sub> and B<sub>2g</sub> components (see Fig. 1a,b) from the XX and X'X' spectra, respectively. As one can see from Fig. 3a,b the A<sub>1g</sub> scattering component peaks in both cases, at  $345\pm 20\text{cm}^{-1}$ . For the crystal with T<sub>c</sub>=90K we found peaks of the B<sub>1g</sub>, A<sub>1g</sub> and B<sub>2g</sub> scattering components at  $460\pm 15\text{cm}^{-1}$ ,  $350\pm 20\text{cm}^{-1}$ , and  $400\pm 35\text{cm}^{-1}$ , respectively (Fig. 4, lower panel).

Another very important observation is that the low frequency behavior of the electronic Raman scattering exhibits strong anisotropy with respect to the symmetry components. One can see in Fig.4a (upper and lower panel) that the intensity decrease of the B<sub>1g</sub> scattering component toward lower frequencies fits the  $\omega^3$  law predicted by Devereaux et al.<sup>27</sup>. For the A<sub>1g</sub> and B<sub>2g</sub> scattering components in Fig. 4b and c, respectively, there is a linear decrease, which also agrees with the predictions by Devereaux et al.<sup>27</sup>. A summary of our results on Tl-2201 is presented in Table I.

In order to follow the temperature behavior of the superconductor gap, we have measured the temperature dependence of the electronic Raman scattering. Following Devereaux et. al.<sup>26,27</sup>, we assume that the peak in the B<sub>1g</sub> component of the electronic scattering corresponds to the value of  $2\Delta_{max}$ . In Fig. 5a and b, respectively, we show the B<sub>1g</sub> and A<sub>1g</sub> scattering component of Tl-2201 (T<sub>c</sub>=80K) at different temperatures between 10K and T<sub>c</sub> divided by the spectrum at 100K. The experiments for the 90-K crystal yielded a similar behavior.

With increasing temperature the intensity of the peak in Fig. 5a associated with the pair breaking process decreases and the maximum shifts slightly to lower frequencies. Obviously, the temperature dependence of the superconductor gap does not follow the BCS behavior. In other words, upon cooling below T<sub>c</sub> the gap opens more abruptly than predicted by BCS theory. These results are similar to results reported for underdoped Bi-2212<sup>22</sup>. Because the peak position of the A<sub>1g</sub> scattering component in Fig. 5b has larger error bars compared to the B<sub>1g</sub> component, one cannot definitely say whether the data fit the BCS behavior or not.

We also searched for superconductivity-induced changes in frequency and linewidth of the optical phonons. With the resolution of  $1\text{cm}^{-1}$  we have not observed such changes. Upon heating from 10K up to 200K the frequencies of all phonons decreased and the linewidths increased monotonically.

### IV. DISCUSSION

The Raman scattering intensity can be written in terms of the differential scattering cross section<sup>27</sup>:

$$\frac{\partial^2 \sigma}{\partial \omega \partial \Omega} = \frac{\omega_s}{\omega_i} r_0^2 S_{\gamma\gamma}(\vec{q}, \omega) \quad (1)$$

with

$$S_{\gamma\gamma}(\vec{q}, \omega) = -\frac{1}{\pi} [1 + n(\omega)] \Im m \chi_{\gamma\gamma}(\vec{q}, \omega) \quad (2)$$

Here  $r_0 = e^2/mc^2$  is the Thomson radius,  $\omega_i(\omega_s)$  is the frequency of incident (scattered) photon,  $\hbar$  and  $k_B$  were set to 1.  $S_{\gamma\gamma}$  is the generalized structure function, which is connected to the imaginary part of the Raman response function  $\chi_{\gamma\gamma}$  through the fluctuation-dissipation theorem;  $n(\omega) = 1/[\exp(\omega/T) - 1]$  is the Bose-Einstein distribution function. The Raman response function can be written as<sup>36</sup>:

$$\chi_{\gamma\gamma}(\vec{q}, \omega) = \langle \gamma_{\vec{k}}^2 \lambda_{\vec{k}} \rangle - \frac{\langle \gamma_{\vec{k}} \lambda_{\vec{k}} \rangle^2}{\langle \lambda_{\vec{k}} \rangle} \quad (3)$$

with the Raman vertex  $\gamma_{\vec{k}}$  written as

$$\gamma_{\vec{k}}(\omega_i, \omega_s) = \sum_L \gamma_L(\omega_i, \omega_s) \Phi_L(\vec{k}), \quad (4)$$

where  $\Phi_L(\vec{k})$  are either Brillouin zone or Fermi surface harmonics<sup>27</sup> which transform according to point group transformations of the crystal and  $\lambda_{\vec{k}}$  is the Tsuneto function:

$$\lambda_{\vec{k}} \propto \frac{|\Delta_{\vec{k}}|^2}{\omega \sqrt{\omega^2 - 4 |\Delta_{\vec{k}}|^2}}. \quad (5)$$

The brackets  $\langle \dots \rangle$  in Eq. 3 denote an average of the momentum  $\vec{k}$  over the Fermi surface.

As is obvious, Raman scattering probes only  $|\Delta|^2$ . Therefore it is not possible to determine whether the gap function changes sign for different directions of  $\vec{k} = (k_x, k_y)$  or not. But nevertheless the symmetry of the gap function can be inferred from the specific spectral features of each symmetry component of the electronic Raman scattering.

For the gap of d-wave symmetry ( $\Delta_{\vec{k}} = \Delta_{max} \cdot \cos 2\phi$ , where  $\phi$  is an angle between  $\vec{k}$  and the a-axis), calculations<sup>26,27</sup> predict different low frequency behavior for the different symmetry components. For  $B_{2g}$  and  $A_{1g}$  scattering components it should show a linear dependence in  $\omega$ , but for  $B_{1g}$  it should be  $\sim \omega^3$ . The appearance of a power law in the low frequency scattering characterizes an energy gap which vanishes on lines on the Fermi surface. An appearance of  $\omega^3$  law in  $B_{1g}$  scattering component is specific for  $d_{x^2-y^2}$ -wave pairing<sup>27</sup>. The predicted values of the peak maxima for the  $B_{1g}$ ,  $B_{2g}$  and  $A_{1g}$  scattering components are  $\sim 2\Delta_{max}$ ,  $\sim 1.6\Delta_{max}$  and  $\sim 1.2\Delta_{max}$ , respectively. These above mentioned peculiarities appear in our data. Indeed, the low frequency behavior of the  $B_{1g}$  scattering component definitely differs from a linear behavior as seen in Fig. 4a, whereas for the  $A_{1g}$  and  $B_{2g}$  scattering components it is linear in  $\omega$  (see Fig. 4b,c). For both crystals, the  $B_{1g}$  scattering component peaks at a higher frequency than the  $B_{2g}$ , which in turn peaks at a higher frequency than the  $A_{1g}$  component.

Since Raman scattering does not probe the phase of the order parameter it is important to take into consideration other types of the pairing which can also have nodes on the Fermi surface, but do not change the sign, i.e.  $s + id$ -pairing, or strongly anisotropic s-pairing. For the  $s + id$ -pairing<sup>27</sup> ( $\Delta(k) = \Delta_s + i\Delta_d \cos 2\phi$ ) one gets the threshold at  $\omega = 2\Delta_s$  (minimum pair breaking energy). While  $A_{1g}$  and  $B_{2g}$  scattering components exhibit a jump at this frequency, the  $B_{1g}$  scattering component shows a continuous rise from zero and up to the peak at  $\omega = 2\Delta_{max} = 2\sqrt{(\Delta_s^2 + \Delta_d^2)}$ . The  $A_{1g}$  and  $B_{2g}$  scattering components also show broad maxima as in the case of pure  $d_{x^2-y^2}$ -wave pairing, but these maxima will be cut-off toward lower frequencies due to the strong jump at  $2\Delta_s$ . Thus one should observe a low-frequency cut-off in both  $A_{1g}$  and  $B_{2g}$  scattering components, which, however, is not observed in our data.

For anisotropic s-pairing, showing the minimum of the gap on the diagonals of the two-dimensional Brillouin zone, ( $\Delta(k) = \Delta_0 + \Delta_1 \cos^4 2\phi$ ) one gets a single threshold on  $2\Delta_0$  for all scattering components as well as a peak at  $\omega = 2\Delta_{max} = 2(\Delta_0 + \Delta_1)$  for the  $B_{1g}$  scattering component. Therefore we will expect a picture which is very similar to the case of  $s + id$ -pairing, with one exception. The  $B_{1g}$  scattering component should show an additional shoulder at the same position where the  $A_{1g}$  and  $B_{2g}$  scattering components show peaks<sup>27</sup>. This is also not the case for our data. In principle one can assume  $\Delta_0$  to be very small or even zero. In this case one gets peaks at  $2\Delta_{max}$ ,  $0.6\Delta_{max}$  and  $0.2\Delta_{max}$  for the  $B_{1g}$ ,  $B_{2g}$  and  $A_{1g}$  scattering components<sup>27</sup>, respectively. In addition, the low frequency behavior of the  $B_{1g}$  scattering component will be linear. This also contradicts our results.

Recently the model calculations of Devereaux et al. were criticized by Krantz and Cardona<sup>29,30</sup>. The main argument against this theoretical model is that the realistic electronic band structure of the crystal is important, but that the one-sheeted Fermi surface approximation used by Devereaux et al.<sup>27</sup> is inappropriate. The authors of Ref. 30 used a numerical model based on the LDA band structure calculations for YBaCuO in order to take into account the multisheeted Fermi surface of the superconductors with several  $\text{CuO}_2$  -planes. It was pointed out that for the  $\Delta = \Delta_0 \cos 2\phi$  (d-wave pairing) and a multisheeted Fermi surface the calculations lead to a contradiction with the experiment, i.e. the  $A_{1g}$  and  $B_{1g}$  scattering components peak at the same position  $2\Delta_0$ . In order to get consistency with the experiment, different types of the order parameter on different sheets of the Fermi surface were proposed. Only in this case the calculations in Ref. 30 were able to get different positions of the maxima of the  $B_{1g}$ ,  $A_{1g}$ , and  $B_{2g}$  scattering components. For a one-sheeted Fermi surface the authors of Ref. 30 found identical positions of the maxima for the  $A_{1g}$  and  $B_{1g}$  components, but a different position for the  $B_{2g}$  component. Hence it was concluded that any difference in peak position of the  $A_{1g}$  and  $B_{1g}$  component is only consistent with multiband scattering of a multisheeted Fermi surface and different gap symmetries for each of the sheets. For superconductors with one  $\text{CuO}_2$ -plane, a multisheeted Fermi surface is invoked originating from Tl-like s-states<sup>30</sup> (Tl-2201) or from Sr-doping<sup>37</sup> ( $\text{La}_{2-x}\text{Sr}_x\text{CuO}_4$ ) in order to yield a difference in peak position for the  $A_{1g}$  and  $B_{1g}$  components. However,

no experimental proof for such a Fermi surface contribution exists so far. Moreover, the calculations in Ref. 30 failed in explaining of the symmetry-dependent low-frequency dependence of the Raman scattering intensity, whereas this important experimental fact was observed not only in our experiments, but also in Bi-Sr-Ca-Cu-O<sup>21,22,26</sup>, Y-Ba-Cu-O<sup>18,19</sup> and La-Sr-Cu-O<sup>25</sup> systems. In addition, it is obvious that all superconductors with different crystal structures have a different electronic structure. Hence, if the multiband scattering model would be crucial we would expect absolutely different behavior for the different superconductors which is actually in contradiction with existing experimental results. Even if one compares the superconductors with the same number of CuO<sub>2</sub> planes, one finds that, while the interplanar distance (distance between Cu atoms in different CuO<sub>2</sub>-planes) is quite similar, the dimpling (in-plane Cu-O-Cu angle) differs very much from compound to compound (see Table II). YBa<sub>2</sub>Cu<sub>3</sub>O<sub>7</sub> exhibits the largest dimpling compared to other compounds. Strong dimpling should lift the degeneracy of otherwise identical CuO<sub>2</sub>-planes or Fermi surface sheets. This dimpling can strongly affect the LDA calculations because the interplanar interaction should depend on this parameter.

And finally on top of that, use of the effective mass approach is very much questionable in case of high temperature superconductors, because this approach can be used only for nonresonant Raman scattering<sup>38</sup>. In high temperature superconductors we, however, are always in the regime of the resonant scattering. Moreover, the electron correlation effects in HTSC are not treated sufficiently by LDA.

In contrast to the conclusion of Ref. 30 our experiments show that the one-CuO<sub>2</sub>-plane compound Tl-2201 shows very similar behavior compared to compounds with several CuO<sub>2</sub>-planes, such as Tl-2223, Bi-2212 and YBaCuO<sup>18-27,29,30</sup>. We also found that the frequency of the B<sub>1g</sub> maximum scales with T<sub>c</sub>, and it corresponds to the value  $2\Delta_{max}/k_B T_c = 7.6 \pm 0.4$ . This value is very close to the values (with the exception of Nd<sub>2-x</sub>Ce<sub>x</sub>CuO<sub>4</sub><sup>11</sup>) found for other high temperature superconductors as shown in Table III.

The temperature dependence of the gap (B<sub>1g</sub> component in Fig. 5a) in our experiment differs from the BCS behavior, i.e. upon cooling the gap opens more abruptly than predicted by BCS theory. This is consistent with the spin fluctuation theory of high temperature superconductivity<sup>39</sup>, favoring d<sub>x<sup>2</sup>-y<sup>2</sup></sub>-wave pairing. The model considers pair binding as well as pair breaking effects due to the spin fluctuations. Gap opening leads to a suppression of low-frequency spin fluctuations and therefore to reduced pair-breaking. Therefore in underdoped crystals (we consider our Tl-2201 crystals as underdoped) this effect will lead to a more abrupt opening of the gap upon cooling below T<sub>c</sub> compared to BCS behavior.

In conclusion, we presented measurements of the electronic Raman scattering on high-T<sub>c</sub> Tl-2201 single crystals with one CuO<sub>2</sub>-plane per unit cell. The peculiarities of the electronic Raman scattering, i.e. the power law frequency dependence of the different scattering components at low frequencies, their different peak positions as well as the values of  $2\Delta_{max}/k_B T_c = 7.6 \pm 0.4$  are found to be very similar in compounds with one and several CuO<sub>2</sub> planes. All nearly optimally doped high-T<sub>c</sub> superconductors (with the exception of (Nd,Ce)-214<sup>11</sup>) show a very similar behavior of the electronic Raman scattering consistent with the d<sub>x<sup>2</sup>-y<sup>2</sup></sub>- wave symmetry of the underlying order parameter.

## V. ACKNOWLEDGMENTS

This work was supported by DFG through SFB 341 and by BMBF FKZ 13 N 6586. One of the authors L.V.G acknowledges support from the Alexander von Humboldt Foundation and expresses his gratitude for the hospitality at the 2.Physikalisches Institut RWTH-Aachen.

---

<sup>1</sup> R.C. Dynes, Solid State Communications 92, 53, (1994).

<sup>2</sup> J.R. Schrieffer, Solid State Communications 92, 129, (1994).

<sup>3</sup> J.M. Valles, Jr., R.C. Dynes, A.M. Cucolo, M. Gurrutxaga, L.F. Schneemeyer, J.P. Garno, J.V. Waszczak, Phys. Rev. B 44, 11986 (1991).

<sup>4</sup> W.N. Hardy, D.A. Bonn, D.C. Morgan, R. Liang, K. Zhang, Phys. Rev. Lett. 70, 3999 (1993).

<sup>5</sup> Y. Kitaoka et al., J. Phys. Chem. Solids 54, 1385 (1993).

<sup>6</sup> C.P. Slichter et al., J. Phys. Chem. Solids 54, 1439 (1993).

<sup>7</sup> Z.Y. Shen, D.S. Dessau, B.O. Wells, D.M. King, W.E. Spicer, A.J. Arko, D. Marshall, L.W. Lombardo, A. Kapitulnik, P. Dickinson, S. Doniach, J. DiCarlo, A.G. Loeser, C.H. Park, Phys. Rev. Lett. 70, 1553 (1993).

<sup>8</sup> J. Ma, C. Quitmann, R.J. Kelley, H. Berger, G. Margaretondo and M. Onellion, preprint.

<sup>9</sup> N. Tralshawala, J.F. Zasadzinski, L. Koffey, Q. Huang, Phys. Rev. B 44, 12102 (1991).

- <sup>10</sup> S.N. Mao et al., Appl. Phys. Lett. 64, 375 (1994).
- <sup>11</sup> B. Stadlober, G. Krug, R. Nemetschek, and R. Hackl, Phys. Rev. Lett. 74, 4911 (1995)
- <sup>12</sup> D.A. Wohlman, D.J. Van Harlinger, W.C. Lee, D.M. Ginsberg, A.G. Leggett, Phys. Rev. Lett. 71, 2134 (1993).
- <sup>13</sup> A.G. Sun, D.A. Gajewski, M.B. Maple, R.C. Dynes, Phys. Rev. Lett. 72, 2267 (1994).
- <sup>14</sup> R. Hackl, R. Kaiser, and S. Schick Tanz, J. Phys. C 16, 1729 (1983)
- <sup>15</sup> S.B. Dierker, M.V. Klein, G.W. Webb, Z. Fisk, Phys. Rev. Lett. 50, 853 (1983)
- <sup>16</sup> K.B. Lyons, M. Hong, H.S. Chen, J. Kwo, T.J. Negrau, Phys. Rev. B 36, 5592 (1987)
- <sup>17</sup> A.V. Bazgenov et al., in Novel Superconductivity, eds. S.A. Wolff and V.S. Kresin ( Plenum Press, New York) 893, (1987).
- <sup>18</sup> R. Hackl, W. Glaser, P. Müller, D. Einzel and K. Anders, Phys. Rev. B 38, 7133 (1988).
- <sup>19</sup> S.L. Cooper, F. Slakey, M.V. Klein, J.P. Rice, E.D. Bukowski, D.M. Ginsberg, Phys. Rev. B 38, 11934 (1988).
- <sup>20</sup> A. Hofmann, P. Lemmens, G. Güntherodt, V. Thomas, K. Winzer, Physica C, 235-240, 1897 (1994).
- <sup>21</sup> T. Stauf er, R. Nemetschek, R. Hackl, P. Müller, and H. Veith, Phys. Rev. Lett. 68, 1069 (1992).
- <sup>22</sup> A. Hoffmann, P. Lemmens, L. Winkler, G. Güntherodt, J. of Low Temp. Phys 99, 201 (1995).
- <sup>23</sup> R. Nemetschek, O.V. Misochko, B. Stadlober and R. Hackl, Phys. Rev. B. 47, 3450 (1993).
- <sup>24</sup> X.K. Chen, E. Altendorf, J.C. Irwin, R. Liang, W.H. Hardy, Phys. Rev. B 48, 10530 (1993).
- <sup>25</sup> X.K. Chen, J.C. Irwin, H.J. Trodahl, T. Kimura, K. Kishio, Phys. Rev. Lett. 73, 3290 (1994).
- <sup>26</sup> T. Devereaux, D. Einzel, B. Stadlober, R. Hackl, D.H. Leach and J.J. Neumeier, Phys. Rev. Lett. 72, 396 (1994).
- <sup>27</sup> T. Devereaux, D. Einzel Phys.Rev. B 51, 16336, (1995).
- <sup>28</sup> T. Devereaux, D. Einzel, private commun.
- <sup>29</sup> M. Krantz and M. Cardona, Phys. Rev. Lett. 72, 3290 (1994).
- <sup>30</sup> M. Krantz and M. Cardona, J. of Low Temp. Physics 99, 205 (1995).
- <sup>31</sup> N.N. Kolesnikov, V.E. Korotkov, M.P. Kulakov, R.P. Shibaeva, V.N.Molchanov, R.A. Tamazyan and V.I. Simonov, Physica C 195, 219 (1992).
- <sup>32</sup> G. Blumberg, M. King, P. Abbamonte, M.V. Klein, M. Karlow, S.L. Cooper, N. Kolesnikov, Physica C 235-240, 1137 (1994).
- <sup>33</sup> Y. Shimakawa, Physica C 202, 199 (1992).
- <sup>34</sup> L.V. Gasparov, V.D. Kulakovskii, O.V. Misochko, A.A. Polyanskii, V.B. Timofeev, Physika C 160, 147 (1989).
- <sup>35</sup> M. Käll, L. Börjesson, C. Ström, S. Eriksson, L.- G. Johansson, Physica C 220, 131 (1994).
- <sup>36</sup> M.V. Klein and S.B. Dierker, Phys. Rev. B 29, 4976 (1984).
- <sup>37</sup> M. Krantz, preprint (1995)
- <sup>38</sup> A.A. Abrikosov and V.M. Genkin, Sov. Phys.-JETP 38, 417 (1974)
- <sup>39</sup> P. Monthoux, A.V. Balatsky, and D. Pines, Phys. Rev. B 46, 14803 (1992).
- <sup>40</sup> J.D. Jorgensen, B.W. Veal, A.P. Paulikas, L.J. Nowicki, G.W. Crabtree, H. Claus, W.K. Kwok, Phys. Rev. B 41, 1866 (1990).
- <sup>41</sup> B. Morosin, D.S. Ginley, P.F. Hlava, M.J. Carr, B.J. Baughman, J.E. Schirber, E.L. Venturini, J.F. Kwak, Physica C 152, 413 (1988).
- <sup>42</sup> M.A. Subramanian, J.C. Calabrese, C.C. Torardi, J. Gopalakrishnan, T.R. Askew, R.B. Flippen, K.J. Morrissey, U. Chowdhry, A.W. Sleight, Nature 332, 420 (1988).
- <sup>43</sup> P. Bordet, J.J. Capponi, C. Chaillout, J. Chenavas, A.W. Hewat, E.A. Hewat, J.L. Hodeau, M. Marezio, J.L. Tholence, D. Tranqui, Physica C 153-155 , 623 (1988).
- <sup>44</sup> R.J. Cava, A. Santoro, J.J. Krajewski, R.M. Fleming, J.V. Wasczak, W.F. Peck Jr., P. Marsh, Physica C 172, 138 (1990).

FIG. 1. Electronic Raman scattering of  $\text{Tl}_2\text{Ba}_2\text{CuO}_{6+\delta}$  ( $T_c=80\text{K}$ ). Shown are spectra at  $T=10\text{K}$  and  $100\text{K}$ , and the divided spectra  $I(T=10\text{K})/I(T=100\text{K})$  for a)  $B_{1g}$  and b)  $B_{2g}$  scattering components. The phonon at  $\sim 490\text{cm}^{-1}$  is due to the leakage of the  $A_{1g}$  scattering component while the other phonons are defect induced infrared activ phonons. Note that the peak in the divided spektrum does not coincide with the phonon at  $\sim 490\text{cm}^{-1}$ . The light polarization is shown in relation to the crystal axes.

FIG. 2. Electronic Raman scattering of  $\text{Tl}_2\text{Ba}_2\text{CuO}_{6+\delta}$  ( $T_c=80\text{K}$ ) in a)  $A_{1g}+B_{2g}$  (XX) and b)  $A_{1g}+B_{1g}$  (X'X') scattering geometries. Shown are spectra at  $T=10\text{ K}$  and  $100\text{ K}$ , and divided spectra  $I(T=10\text{K})/I(T=100\text{K})$ . The phonon at  $\sim 490\text{cm}^{-1}$  was cut off in order to show the variations of electronic Raman scattering. The polarization is shown in relation to the crystal axes.

FIG. 3. Electronic Raman scattering of  $\text{Tl}_2\text{Ba}_2\text{CuO}_{6+\delta}$  in  $A_{1g}$  scattering geometry evaluated from a) XX and b) X'X' spectra. Shown are spectra at  $T=10\text{ K}$  and  $100\text{ K}$ , and divided spectra  $I(T=10\text{K})/I(T=100\text{K})$ . The phonon at  $\sim 490\text{cm}^{-1}$  was cut off in order to show the changes of electronic Raman scattering.

FIG. 4. Electronic Raman scattering in Tl-2201 with  $T_c=80$  (upper panel) and  $90\text{K}$  (lower panel). Shown are divided spectra  $I(T=10\text{K})/I(T=100\text{K})$  for a)  $B_{1g}$ , b)  $A_{1g}$  and c)  $B_{2g}$  scattering components.

FIG. 5. Temperature dependence of the electronic Raman scattering. Shown are spectra for  $10, 35$  and  $50\text{K}$  (upper panel), and values of  $\Delta(T)/\Delta_0$  (lower panel) evaluated for a)  $B_{1g}$  and b)  $A_{1g}$  scattering components. In the lower panel the temperature dependence of the peak positions is compared to that of the BCS theory

TABLE I. Peak positions of the different scattering components of electronic Raman scattering. The reduced gap values  $2\Delta/k_B T_c$  are referred to the  $B_{1g}$  peak position, n is the number of  $\text{CuO}_2$ -planes per unit cell.

Compound	n	$T_c$ [K]	$B_{1g}$ [ $\text{cm}^{-1}$ ]	$A_{1g}$ [ $\text{cm}^{-1}$ ]	$B_{2g}$ [ $\text{cm}^{-1}$ ]	$2\Delta/k_B T_c$
$\text{Tl}_2\text{Ba}_2\text{CuO}_6$	1	90	$460\pm 15$	$350\pm 20$	$400\pm 35$	$7.4\pm 0.4$
$\text{Tl}_2\text{Ba}_2\text{CuO}_6$	1	80	$430\pm 15$	$345\pm 35$	$380\pm 35$	$7.8\pm 0.4$

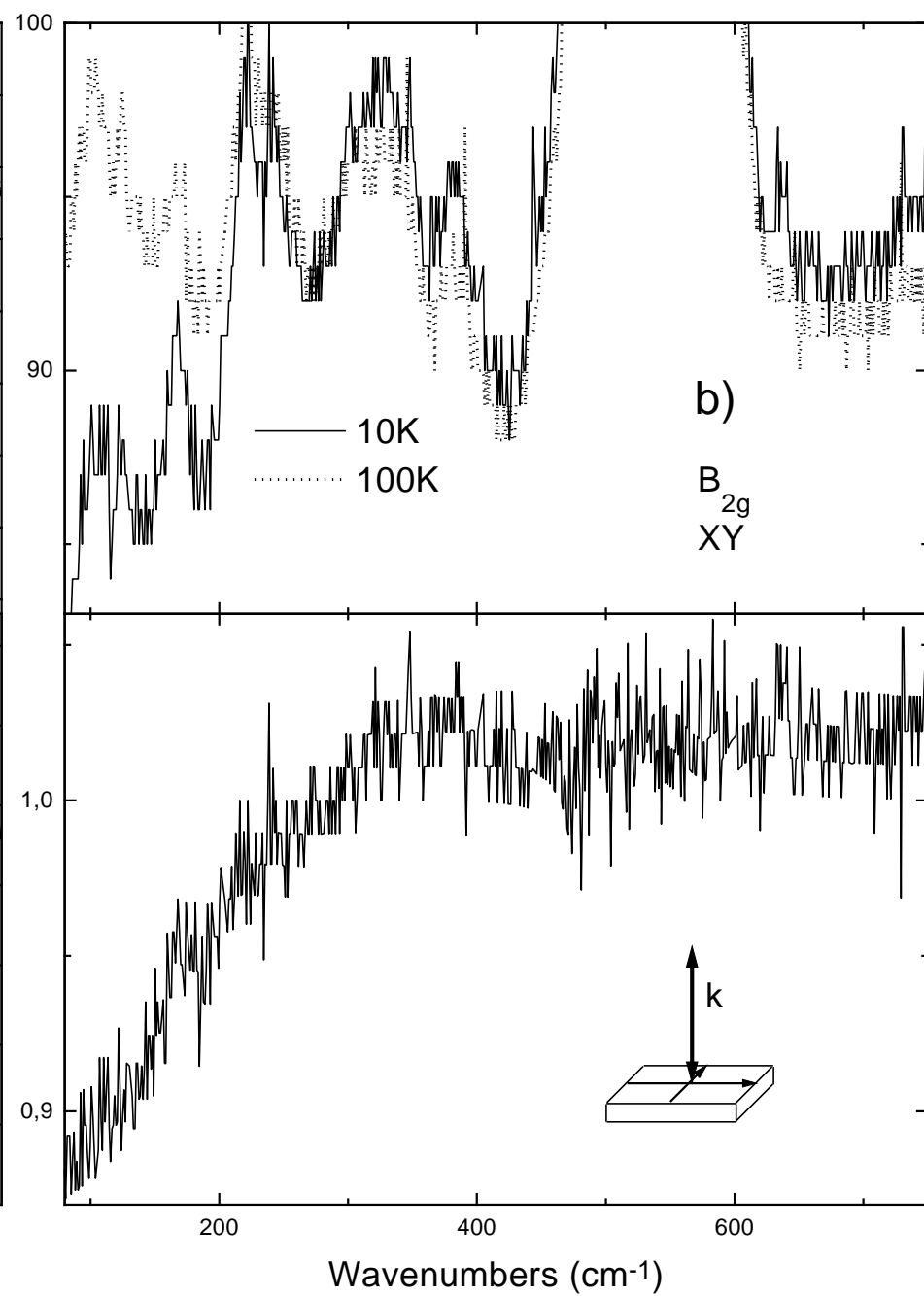
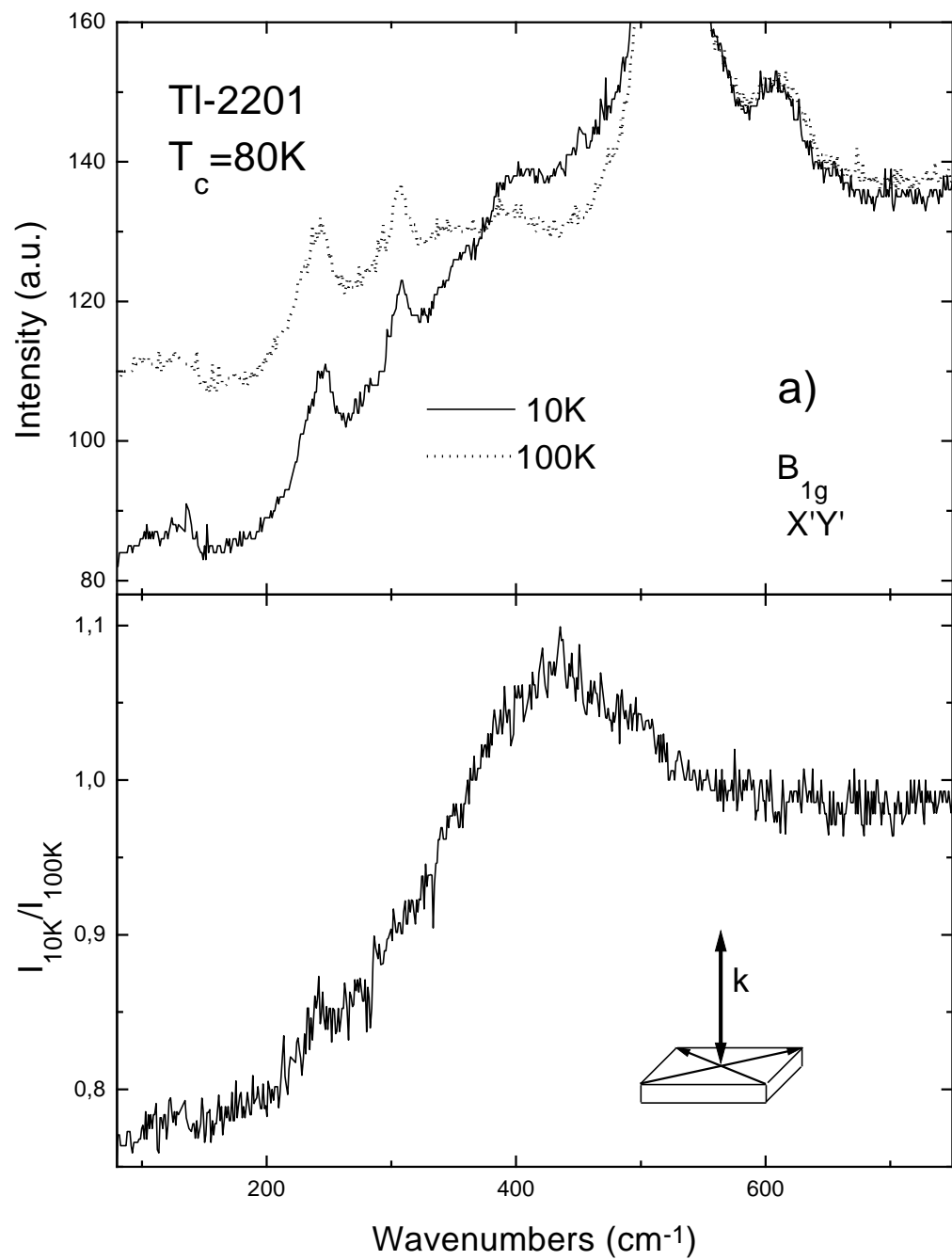
TABLE II. Interplanar Cu-Cu distance and dimpling (Cu-O-Cu angle in  $\text{CuO}_2$ -plane) for different high temperature superconductors with two (n=2)  $\text{CuO}_2$  planes per unit cell.

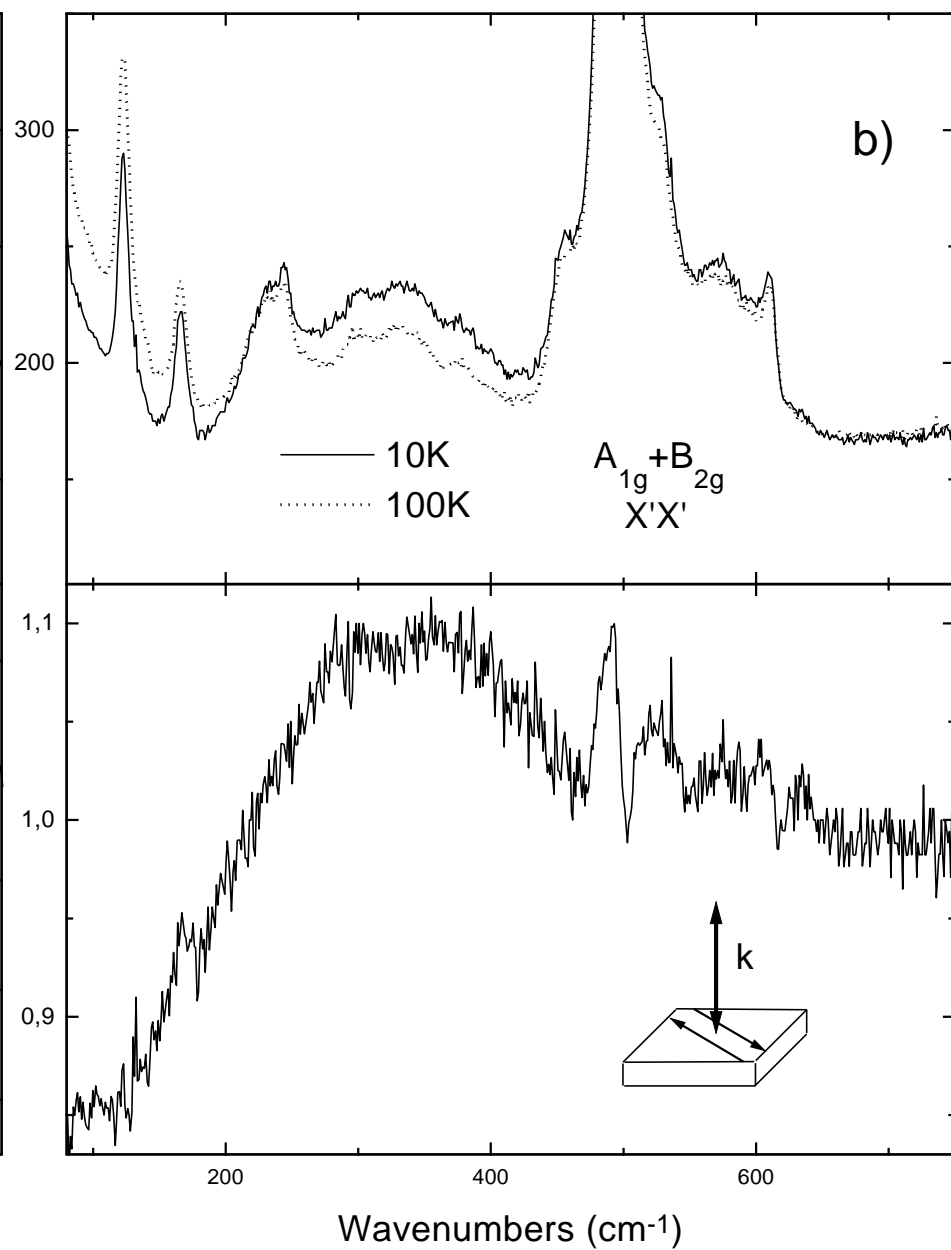
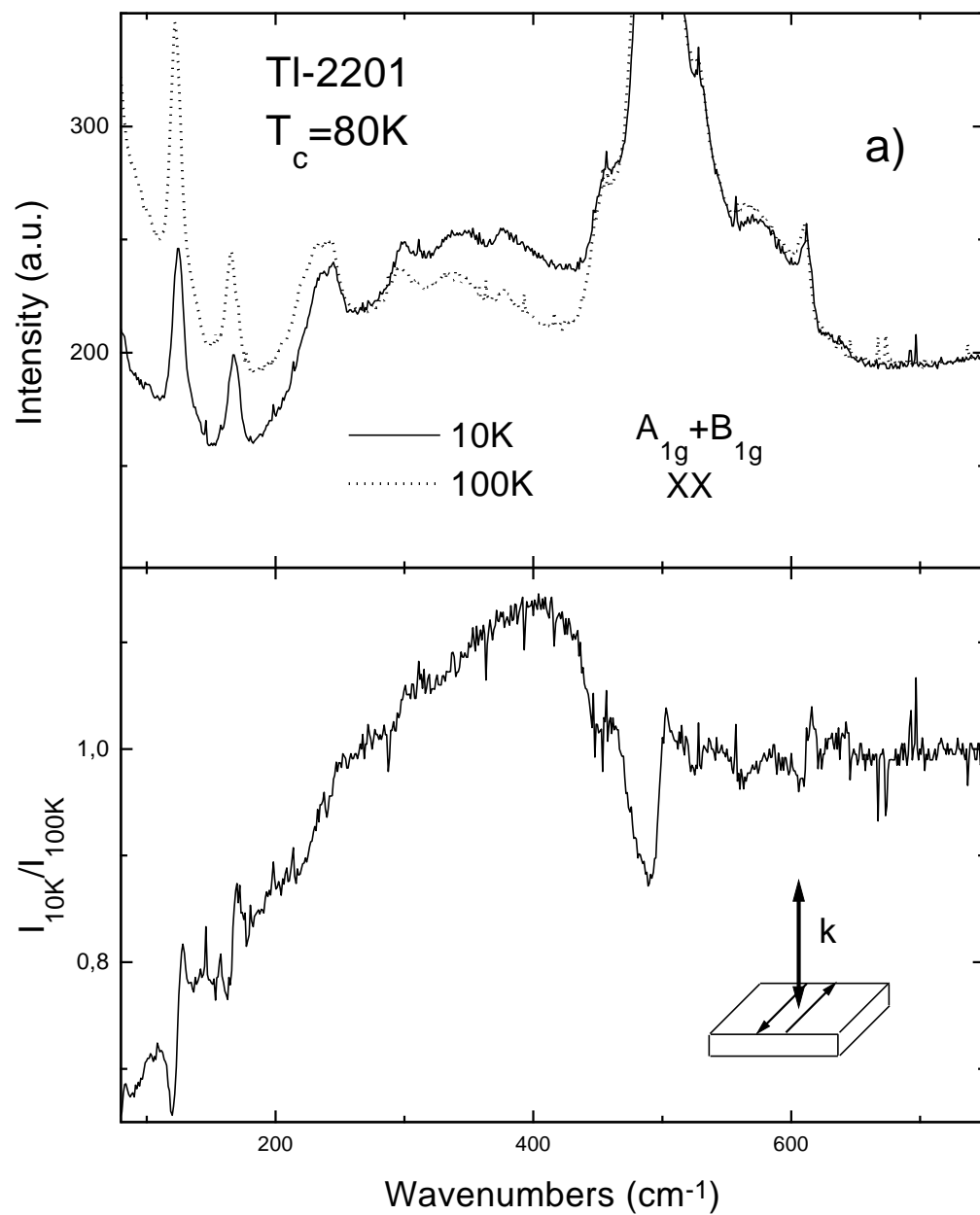
Compound	n	$T_c$ [K]	interplane distance [ $\text{\AA}$ ]	dimpling [deg]
$\text{YBa}_2\text{Cu}_3\text{O}_{7-\delta}$ <sup>40</sup>	2	92	3.37	164
$\text{TlBa}_2\text{CaCu}_2\text{O}$ <sup>41</sup>	2	103	3.20	177
$\text{Tl}_2\text{Ba}_2\text{CaCu}_2\text{O}_8$ <sup>42</sup>	2	110	3.17	178
$\text{Bi}_2\text{Sr}_2\text{CaCuO}_8$ <sup>43</sup>	2	84	3.44	179
$\text{La}_{1.6}\text{Sr}_{0.4}\text{CaCu}_2\text{O}_{5.94}$ <sup>44</sup>	2	55	3.40	175

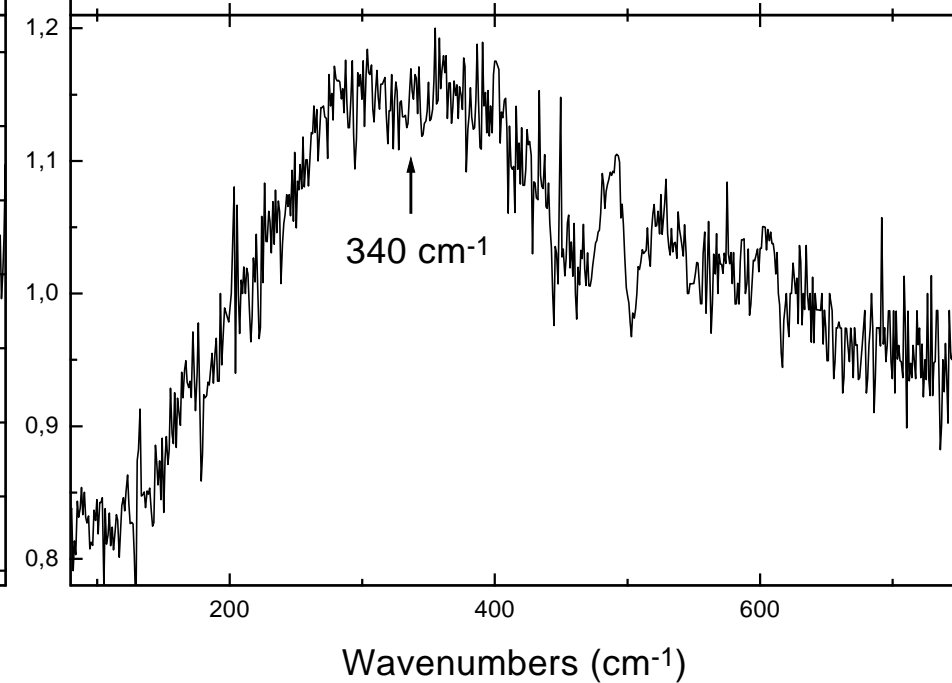
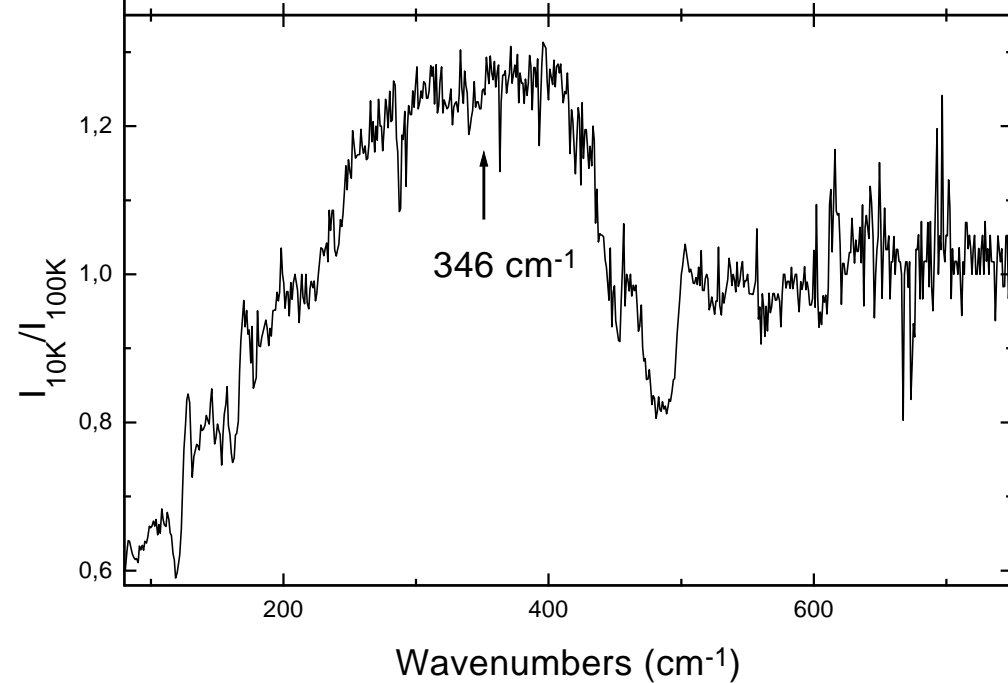
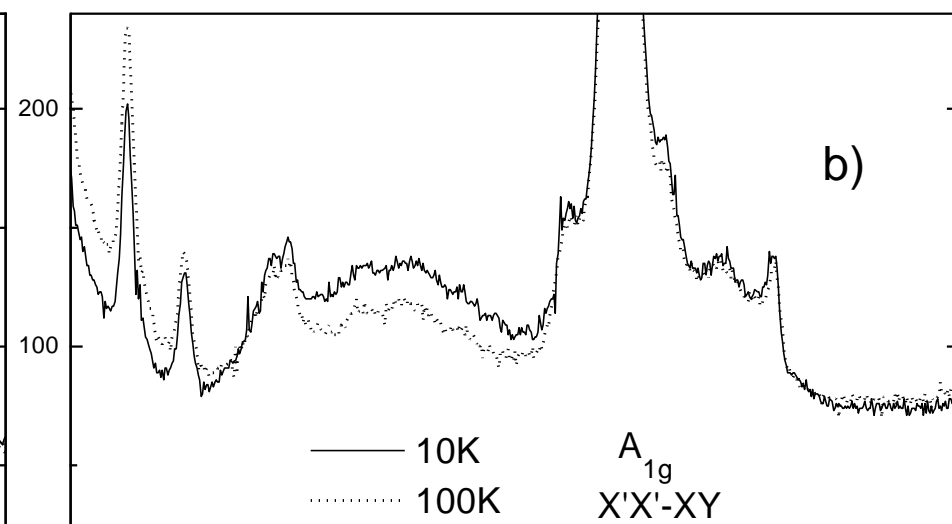
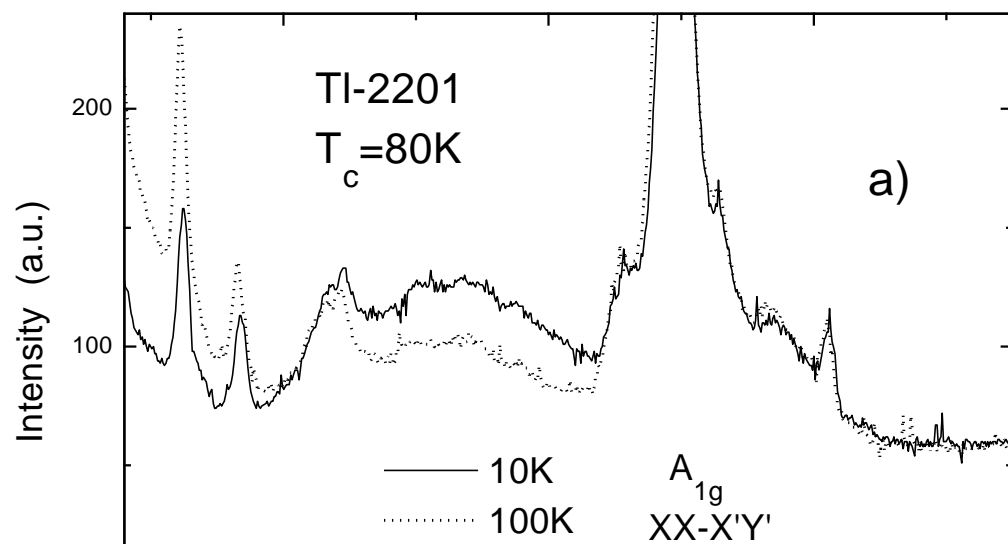
TABLE III. Peak positions of the different symmetry components and reduced gap values  $2\Delta/k_B T_c$  for different investigated high temperature superconductors with different number n of  $\text{CuO}_2$  planes per unit cell.

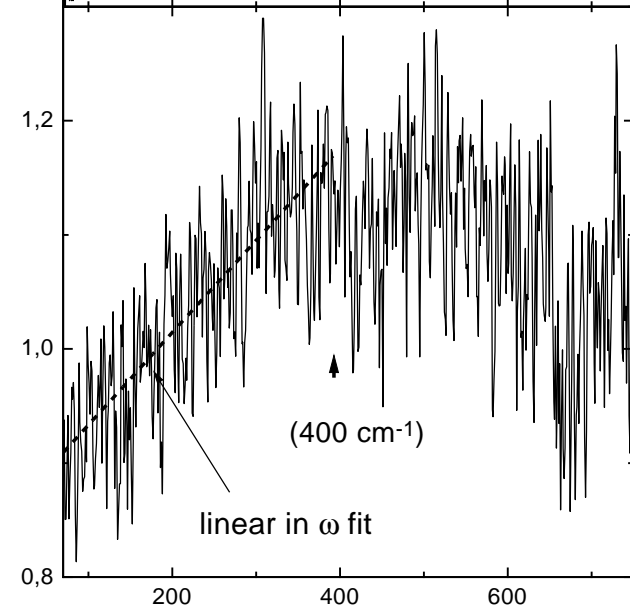
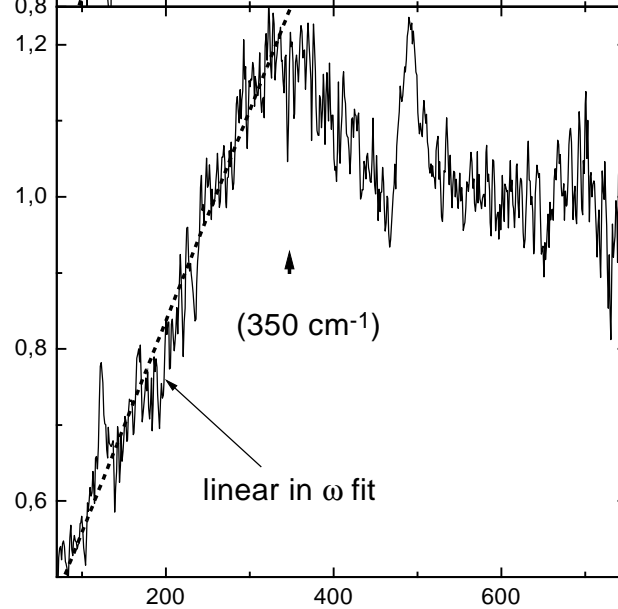
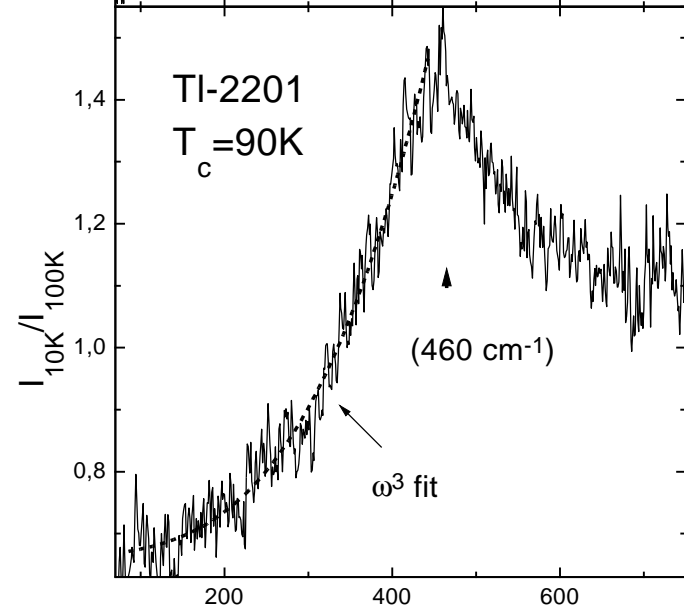
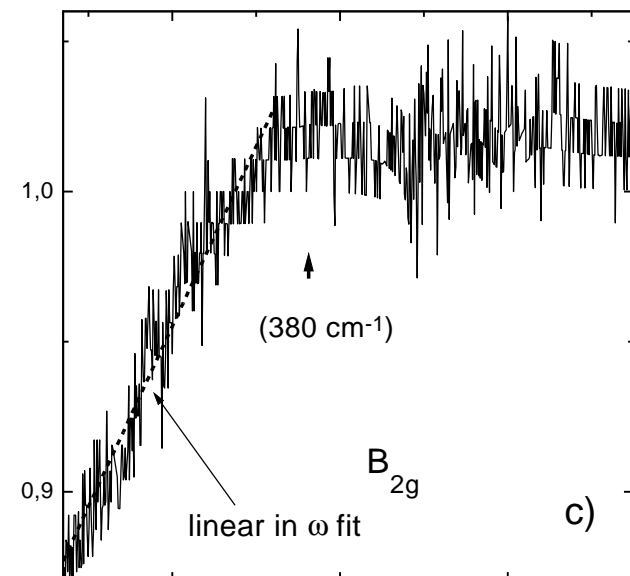
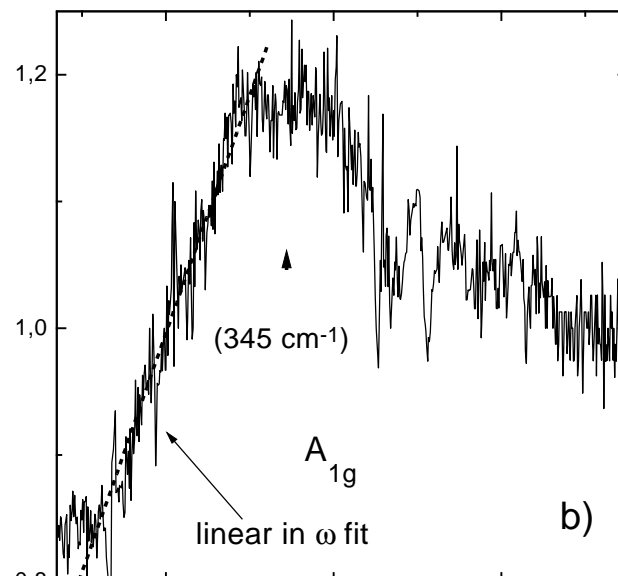
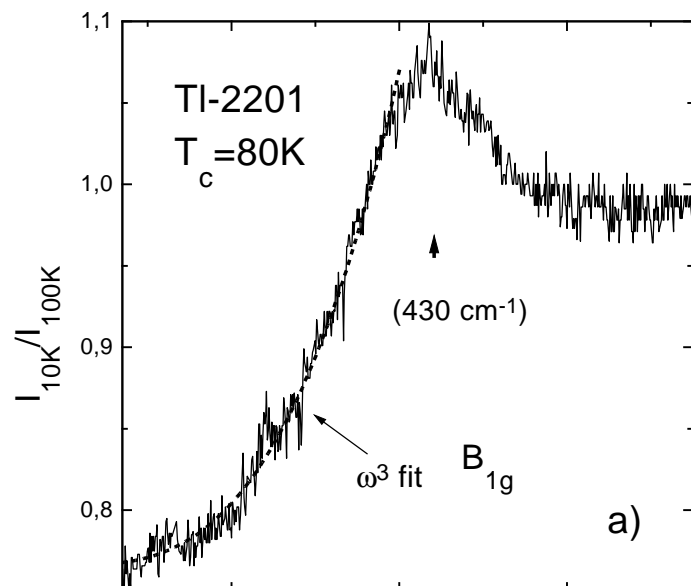
Compound	n	$T_c$ [K]	$B_{1g}$ [ $\text{cm}^{-1}$ ]	$A_{1g}$ [ $\text{cm}^{-1}$ ]	$2\Delta/k_B T_c$
$\text{YBa}_2\text{Cu}_3\text{O}_{7-\delta}$ <sup>24</sup>	2	89.7	420	310	7.6
		93.7	550	310	8.4
$\text{Bi}_2\text{Sr}_2\text{CaCuO}_8$ <sup>22</sup>	2	81	460	280	8.2
		86	520	330	8.7
$\text{La}_{2-x}\text{Sr}_x\text{CuO}_4$ <sup>25</sup>	1	37	200	125	7.8
$\text{Tl}_2\text{Ba}_2\text{Ca}_2\text{Cu}_3\text{O}_{10}$ <sup>20</sup>	3	118	610	430	7.5
$\text{Nd}_{2-x}\text{Ce}_x\text{CuO}_4$ <sup>11</sup>	1	19.3	70	70	5.2











Wavenumbers ( $\text{cm}^{-1}$ )

